Journal of Thermal Analysis, Vol. 37 (1991) 1533-1543

Dedicated to Prof. Dr. H. J. Seifert on the occasion of his 60th birthday

KINETICS AND MECHANISM OF THERMAL DECOMPOSITION OF INSITU GENERATED CALCIUM CARBONATE

K. N. Ninan, K. Krishnan and V. N. Krishnamurthy

PROPELLANTS POLYMERS AND CHEMICALS, VIKRAM SARABHAI SPACE CENTRE, TRIVANDRUM 22, INDIA

(Received December 10, 1990)

Thermogravimetric studies on two varieties of calcium carbonate viz., analytical reagent-grade and insitu generated from calcium oxalate monohydrate, were carried out. The kinetics and mechanism of their solid-state thermal decomposition reaction were evaluated from the TG data using integral methods and the effect of procedural factors such as heating rate, sample mass and method of computation on them were also studied. The procedural variables in the range studied had no marked influence on the results; however the kinetic parameters were marginally higher for the insitu generated calcium carbonate. This trend is explained by the presence of more micropores in the insitu generated calcium carbonate as well as the mechanism of its decomposition following phase boundary reaction with cylindrical symmetry.

The thermal decomposition of calcium carbonate has been extensively studied over the years [1, 2]. It is a high temperature reversible decomposition reaction involving a relatively large mass-loss associated with the evolution of carbon dioxide and hence used as a model reaction for the study of the influence of many experimental variables. A number of TG studies dealing with the kinetics and mechanism of the thermal decomposition of calcium carbonate have been reported [3–7]. The kinetic parameters viz., energy of activation E and preexponential factor A for the reaction, were found to be influenced by experimental conditions such as heating rate, sample mass, furnace atmosphere and the partial pressure of carbon dioxide.

Widely varying values (E = 40 to 900 kcal·mol^{-1} and A = 10^4 to 10^{157}s^{-1}) have been reported under varying experimental conditions [3–5]. Empirical

John Wiley & Sons, Limited, Chichester
Akadémiai Kiadó, Budapest

correlations between kinetic parameters and sample mass have also been reported [3]. However, some authors attribute these variations to the calculation procedure employed and report more or less constant value of E and A, independent of procedural factors such as heating rate [7]. Different reaction mechanisms based on three dimensional diffusion, contracting area and contracting cube have also been proposed [3, 7].

Due to these raging controversies, it was considered worthwhile to reinvestigate the problem, adding a new dimension in the form of the role of in-situ generated sample on the kinetics and mechanism of solid-state thermal decomposition of calcium carbonate. A comparison was made between the analytical reagent-grade commercial sample and insitu produced calcium carbonate from calcium oxalate monohydrate. Attempted also was the study of the influence of procedural variables viz., heating rate and sample mass on the thermal decomposition of these two types of samples.

Experimental

Samples

i. Calcium carbonate ($CaCO_3$)– analytical reagent-grade, BDH.

ii. Calcium oxalate monohydrate ($CaC_2O_4 \cdot H_2O$), Dupont USA, TG calibration standard.

TG experiments

All thermogravimetric (TG) experiments were carried out in 50 $ml \cdot min^{-1}$ flowing nitrogen (99.9% pure) using the Dupont 990 modular thermal analysis system in conjunction with 951 thermogravimetric analyzer. The experiments were conducted at six heating rates (2, 5, 10, 20, 50 and 100 $deg \cdot min^{-1}$) at a constant sample mass of 10 ± 0.1 mg. To study the effect of sample mass, the heating rate was kept constant at 10 $deg \cdot min^{-1}$ and the mass varied from 2.5 to 20 mg (six sets).

Scanning electron micrographs of AR calcium carbonate and insitu generated calcium carbonate were taken using a Steroscan 250 MK3 model SEM from Cambridge Instruments.

Kinetic calculations were done with a CDC computer, using FORTRAN IV program.

Results and discussion

Kinetic parameters

The non-isothermal kinetic analysis is based on the general rate equation:

$$\frac{d\alpha}{f(\alpha)} = \frac{A}{\Phi} \cdot e^{-(E/RT)}\, dT \tag{1}$$

where α = fraction decomposed at temperature T, Φ = heating rate and R = gas constant. The integral method is generally accepted as the more accurate method for the evaluation of the activation parameters from TG data [8]. In the non-mechanistic approach $f(\alpha)$ is taken as $(1-\alpha)^n$, where n = order parameter, so that the integral form of the LHS of Eq. (1) becomes $g(\alpha) = \left[1-(1-\alpha)^{1-n}\right]/(1-n)$ for all values of n except $n=1$, for which $g(\alpha) = -\ln(1-\alpha)$.

The reaction order parameter n was first determined by an iteration method described earlier [9], using the Coats–Redfern Eq. (10). The best fit value of n was found to be 0.5 in almost all the cases. Using this value, the kinetic parameters E and A were computed with the following four non-mechanistic integral equations.

Coats–Redfern (CR) Eq. (10)

$$\ln\left[\frac{1-(1-\alpha)^{1-n}}{(1-n)T^2}\right] = \ln\left[\frac{AR}{\Phi E}\left(1-\frac{2RT}{E}\right)\right] - \frac{E}{RT} \tag{2}$$

Madhusudanan–Krishnan–Ninan (MKN) Eq. (11).

$$\ln\left[\frac{1-(1-\alpha)^{1-n}}{(1-n)T^{1.9215}}\right] = \ln\frac{AE}{\Phi R} + 3.7721 - 1.9215\ln E - \frac{0.12039E}{T} \tag{3}$$

MacCallum–Tanner (MT) Eq. (12)

$$\log\left[\frac{1-(1-\alpha)^{1-n}}{(1-n)}\right] = \log\frac{AE}{\Phi R} - 0.483E^{0.435} - \frac{(0.449+0.217E)\cdot 10^3}{T} \tag{4}$$

Horowitz–Metzger (HM) Eq. (13)

$$\ln\left[\frac{1-(1-\alpha)^{1-n}}{(1-n)}\right] = \ln\frac{ART_s^2}{\Phi E} - \frac{E}{RT_s} + \frac{E\Theta}{RT_s^2} \tag{5}$$

where T_S = DTG peak temperature and $\Theta = T - T_S$

The LHS off Eqs (2–4) were plotted against the reciprocal of absolute temperature ($1/T$) and for Eq. (5) against Θ. A typical Coast-Redfern plot for the two samples is given in Fig. 1. The values of E and A were computed from the slope and intercept respectively. These values along with the correlation coefficients, for each curves are given in Tables 1 to 4.

Tables 1 and 2 summarize the results obtained at six heating rates for the two types of samples and Tables 3 and 4 give the results for six sample mass. In all the 96 kinetic curves the correlation coefficients are above 0.999 indicating good linearity. From these tables, it can also be observed that the Horowitz–Metzger equation gives higher values of E and A and relatively lower correlation coefficients for all the cases. This is because of the inherent error involved in the approximation method employed in the derivation of the HM equation . The remaining three 'exact integral' equation give results in close agreement, the best agreement resulting from the CR and MKN equation .

Table 1 Effect of heating rate on kinetic data for thermal decomposition of AR $CaCO_3$ from non-mechanistic equations

Heating rate	Equations					
	Coats–Redfern			Madhusudanan–Krishnan–Ninan		
Φ	E	A	r	E	A	r
2	43.07	$5.21 \cdot 10^6$	0.9998	43.35	$8.28 \cdot 10^6$	0.9999
5	43.05	$1.18 \cdot 10^7$	0.9998	43.26	$2.25 \cdot 10^7$	0.9999
10	43.35	$7.38 \cdot 10^6$	0.9998	43.84	$1.39 \cdot 10^7$	0.9998
20	43.36	$4.36 \cdot 10^6$	0.9998	43.57	$8.25 \cdot 10^6$	0.9998
50	43.10	$5.83 \cdot 10^6$	0.9999	43.33	$1.01 \cdot 10^7$	0.9999
100	42.98	$3.27 \cdot 10^6$	0.9991	43.21	$5.77 \cdot 10^6$	0.9992
	MacCallum–Tanner			Horowitz–Metzger		
2	44.93	$2.10 \cdot 10^7$	0.9999	50.84	$3.41 \cdot 10^8$	0.9994
5	46.42	$5.12 \cdot 10^7$	0.9998	52.69	$9.04 \cdot 10^8$	0.9996
10	45.68	$3.38 \cdot 10^7$	0.9998	51.98	$5.33 \cdot 10^8$	0.9994
20	45.72	$2.19 \cdot 10^7$	0.9998	52.24	$3.18 \cdot 10^8$	0.9991
50	45.51	$3.05 \cdot 10^7$	0.9999	51.98	$3.83 \cdot 10^8$	0.9994
100	45.15	$4.89 \cdot 10^6$	0.9991	52.10	$4.63 \cdot 10^7$	0.9996

$\Phi = \text{deg} \cdot \text{min}^{-1}$, $E = \text{kcal} \cdot \text{mol}^{-1}$ and $A = \text{s}^{-1}$

Reaction mechanism

The kinetic parameters were also calculated using the mechanism based equation from the TG data. In the mechanism based kinetic equation, a series of $f(\alpha)$ forms are proposed for the solid-state decomposition reactions governed by different mechanism such as nucleation, diffusion and

Table 2 Effect of heating rate on kinetic data for thermal decomposition of insitu $CaCO_3$ from non-mechanistic equations

Heating rate	Equations					
	Coats–Redfern			Madhusudanan–Krishnan–Ninan		
Φ	E	A	r	E	A	r
2	43.91	$1.87 \cdot 10^7$	0.9996	44.12	$3.64 \cdot 10^7$	0.9997
5	44.36	$1.02 \cdot 10^7$	0.9998	44.86	$2.53 \cdot 10^7$	0.9998
10	44.91	$2.93 \cdot 10^7$	0.9998	45.20	$5.57 \cdot 107$	0.9999
20	44.34	$1.56 \cdot 10^7$	0.9999	44.55	$3.02 \cdot 107$	0.9999
50	44.67	$1.72 \cdot 10^7$	0.9990	44.79	$3.21 \cdot 107$	0.9992
100	43.96	$1.13 \cdot 10^7$	0.9995	44.22	$3.16 \cdot 10^7$	0.9996
	MacCallum–Tanner			Horowitz–Metzger		
2	45.74	$7.14 \cdot 10^7$	0.9997	51.74	$1.43 \cdot 10^9$	0.9994
5	44.98	$4.12 \cdot 10^7$	0.9998	51.03	$7.03 \cdot 10^8$	0.9994
10	46.89	$1.29 \cdot 10^8$	0.9998	53.17	$2.36 \cdot 10^9$	0.9994
20	46.55	$7.48 \cdot 10^7$	0.9999	52.53	$9.18 \cdot 10^8$	0.9990
50	47.08	$9.08 \cdot 10^7$	0.9991	53.06	$9.25 \cdot 10^8$	0.9989
100	46.46	$6.27 \cdot 10^7$	0.9996	52.79	$6.59 \cdot 10^8$	0.9980

phase boundary reactions. Nine probable reaction mechanisms listed by Satava [14] and the temperature integral of the RHS of Eq. (1), which is an incomplete gamma function, used in the form given by Coats and Redfern [10] were employed for the kinetic calculations. The forms of $g(\alpha)$ and the corresponding rate controlling process for the nine reaction mechanisms are given in Table 5. The mechanism of the reaction is obtained from the equation which gives best linear curve, i.e. the highest value of the correlation coefficient. In the cases where more than one equation gives linear curves, the reaction mechanism is chosen from the function $g(\alpha)$ which gives kinetic parameters in agreement with the corresponding non-mechanistic method, as suggested by Fong and Chen [15].

All the 24 sets of TG data were analyzed with the nine equations and the reaction mechanism was chosen from the 216 kinetic curves by applying the above two criteria. In the present case, it is observed that the reaction follows the mechanism of a phase boundary reaction with cylindrical symmetry, representing the contracting area equation :

$$1 - (1 - \alpha)^{1/2} = kt \qquad (6)$$

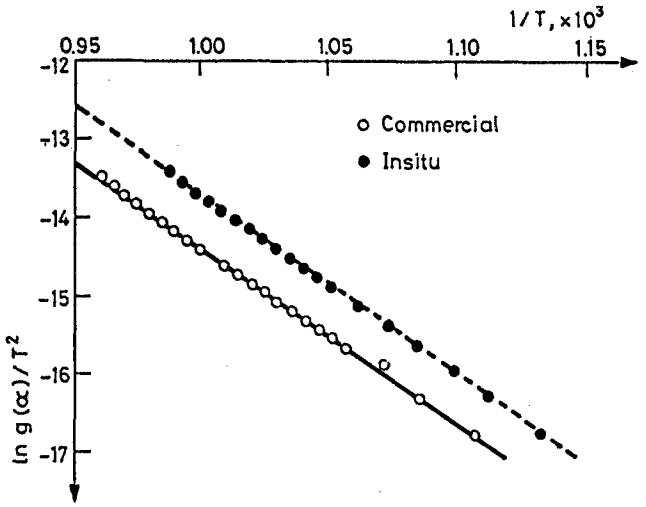

Fig. 1 Coats–Redfern kinetic plot for $CaCO_3$ (sample mass = 10 mg, $\Phi = 10^{\circ}C$)

Table 3 Effect of sample mass on kinetic data for thermal decomposition of AR $CaCO_3$ from non-mechanistic equations

Mass,	Equations					
mg	Coats–Redfern			Madhusudanan–Krishnan–Ninan		
m	*E*	*A*	*r*	*E*	*A*	*r*
2.5	48.78	$1.01 \cdot 10^8$	0.9997	49.07	$2.11 \cdot 10^8$	0.9997
5.0	49.43	$1.55 \cdot 10^8$	0.9993	49.70	$3.15 \cdot 10^8$	0.9996
7.5	44.53	$1.45 \cdot 10^7$	0.9997	44.79	$3.35 \cdot 10^7$	0.9998
10.0	43.55	$9.38 \cdot 10^6$	0.9998	43.86	$1.92 \cdot 10^7$	0.9999
15.0	45.39	$1.67 \cdot 10^7$	0.9998	45.68	$3.24 \cdot 10^7$	0.9998
20.0	44.98	$1.11 \cdot 10^7$	0.9999	45.21	$2.12 \cdot 10^7$	0.9999
	MacCallum–Tanner			Horowitz–Metzger		
2.5	51.24	$8.51 \cdot 10^8$	0.9997	58.15	$1.23 \cdot 10^{10}$	0.9990
5.0	51.67	$7.83 \cdot 10^8$	0.9995	58.31	$3.19 \cdot 10^{10}$	0.9991
7.5	46.68	$3.38 \cdot 10^7$	0.9998	53.06	$1.12 \cdot 10^9$	0.9996
10.0	45.70	$6.62 \cdot 10^7$	0.9998	52.08	$6.33 \cdot 10^8$	0.9994
15.0	47.59	$8.02 \cdot 10^7$	0.9998	53.80	$1.14 \cdot 10^9$	0.9996
20.0	47.20	$5.35 \cdot 10^7$	0.9999	53.53	$7.69 \cdot 10^8$	0.9992

where k = specific rate constant and t = time.

Table 4 Effect of sample mass on kinetic data for thermal decomposition of insitu $CaCO_3$ from non-mechanistic equations

Mass,	Equations					
mg	Coats–Redfern			Madhusudanan–Krishnan–Ninan		
m	E	A	r	E	A	r
2.5	50.19	$3.35 \cdot 10^9$	0.9997	50.48	$6.45 \cdot 10^9$	0.9997
5.0	49.95	$6.59 \cdot 10^8$	0.9998	50.26	$1.49 \cdot 10^9$	0.9999
7.5	45.25	$4.25 \cdot 10^7$	0.9998	45.48	$8.54 \cdot 10^7$	0.9998
10.0	44.91	$2.93 \cdot 10^8$	0.9996	45.17	$6.11 \cdot 10^8$	0.9997
15.0	50.24	$2.92 \cdot 10^8$	0.9993	50.45	$6.35 \cdot 10^8$	0.9994
20.0	50.02	$1.55 \cdot 10^8$	0.9993	50.29	$3.30 \cdot 10^8$	0.9996
	MacCallum–Tanner			Horowitz–Metzger		
2.5	52.65	$8.49 \cdot 10^9$	0.9997	58.76	$2.10 \cdot 10^{10}$	0.9993
5.0	51.24	$8.51 \cdot 10^8$	0.9998	57.36	$1.58 \cdot 10^9$	0.9992
7.5	47.78	$1.87 \cdot 10^8$	0.9997	53.10	$2.57 \cdot 10^9$	0.9990
10.0	46.92	$1.29 \cdot 10^8$	0.9998	53.20	$2.34 \cdot 10^{10}$	0.9994
15.0	52.46	$1.47 \cdot 10^9$	0.9999	58.17	$6.48 \cdot 10^{10}$	0.9990
20.0	51.65	$7.83 \cdot 10^8$	0.9995	56.50	$1.23 \cdot 10^{10}$	0.9989

The E and A values obtained from the non-mechanistic equations are in good agreement with those from the contracting area equation. Tables 6 and 7 summarize the kinetic parameters computed from Eq. (6) for the two samples. Table 6 shows the effect of heating rate and Table 7 that of sample mass. From the tables giving the kinetic results, it can be noted that the kinetic parameters are more or less steady, except at certain extremities, almost unaffected by heating rate, sample mass or the method of computation. A statistical analysis (mean, standard deviation and coefficient of variation) was performed with the data and the results are given in Table 8. The observations made from this study are:

1. The computed values of E are unaffected by either mechanistic or non-mechanistic equations for a given experimental data (the exception of HM equation has been explained earlier).

2. The deviation caused by heating rate is smaller in comparison to that by the sample mass.

Table 5 Commonly used $g(\alpha)$ forms for solid-state reactions (14)

Eqn. No.	Form of $g(\alpha)$	Rate-controlling process
1	α^2	One-dimensional diffusion
2	$\alpha + (1-\alpha)\ln(1-\alpha)$	Two-dimensional diffusion
3	$[1-(1-\alpha)^{1/3}]^2$	Three-dimensional diffusion, spherical symmetry, Jander equation
4	$(1-\frac{2}{3}\alpha) - (1-\alpha)^{2/3}$	Three-dimensional diffusion, spherical symmetry, Ginstling–Brounshtein equation
5	$-\ln(1-\alpha)$	Random nucleation, one nucleus on each particle, Mampel equation
6	$[-\ln(1-\alpha)]^{1/2}$	Random nucleation, Avrami equation I
7	$[-\ln(1-\alpha)]^{1/3}$	Random nucleation, Avrami equation II
8	$1-(1-\alpha)^{1/2}$	Phase boundary reaction, cylindical symmetry
9	$1-(1-\alpha)^{1/3}$	Phase boundary reaction, spherical symmetry

Table 6 Effect of heating rate on kinetic data for thermal decomposition of $CaCO_3$ from contracting area equations

	AR $CaCO_3$			Insitu $CaCO_3$		
Φ	E	A	r	E	A	r
2	43.07	$2.60 \cdot 10^6$	0.9998	43.91	$9.33 \cdot 10^6$	0.9996
5	43.05	$5.98 \cdot 10^6$	0.9998	44.36	$1.02 \cdot 10^7$	0.9998
10	43.55	$3.69 \cdot 10^6$	0.9998	44.91	$1.47 \cdot 10^7$	0.9998
20	43.36	$2.18 \cdot 10^6$	0.9998	44.34	7.79·106	0.9998
50	40.10	$2.19 \cdot 10^6$	0.9999	44.67	8.62·106	0.9992
100	42.98	$2.43 \cdot 10^6$	0.9991	43.96	$5.66 \cdot 10^6$	0.9995

3. All the deviations caused by both heating rate and sample mass are within permissible limits [16]. From this we can infer that the dependence of kinetic parameters on experimental variables such as heating rate and sample mass is not significant.

4. For all the sets of results, the E values of insitu generated calcium carbonate are marginally higher. From this we can infer that the sample history has a definite effect on the computed values of E, even though the magnitude of the effect is very small. This observation can be explained as follows. In the phase boundary reaction the surface nucleation is instantaneous

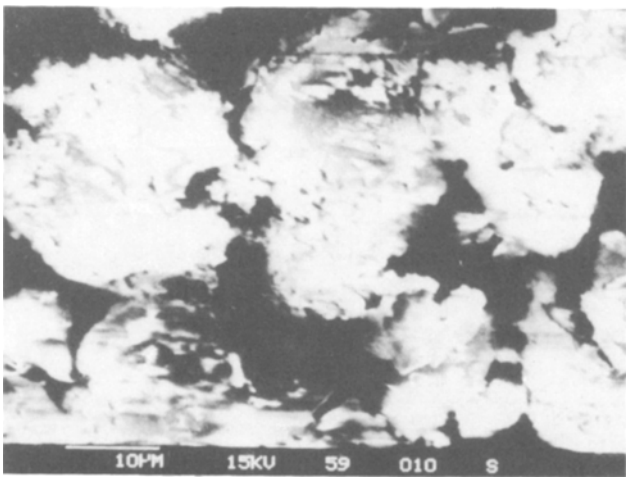

Fig. 2a SEM photographs of $CaCO_3$; insitu generated $CaCO_3$

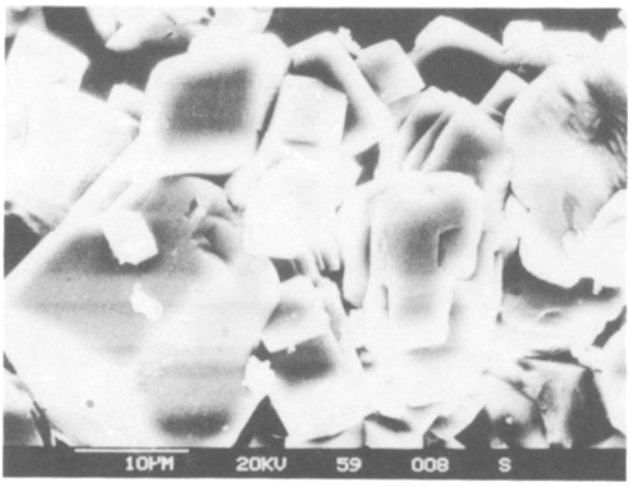

Fig. 2b SEM photographs of $CaCO_3$; analytical reagent-grade $CaCO_3$

and hence the rate controlling process is the movement of the interface towards the interior. Thus, even though the number of nucleation sites for the two types of samples are likely to be largely different, it will have no effect on the reaction rate. However, the marginal increase in kinetic parameters for the insitu produced $CaCO_3$ can be attributed to the larger number of micropores in this sample (Fig. 2). These pores lead to longer

Table 7 Effect of sample mass on kinetic data for thermal decomposition of Ca CO_3 from contracting area equations

Mass,	AR $CaCO_3$			Insitu CaCO3		
mg	E	A	r	E	A	r
2.5	48.78	$7.24 \cdot 10^7$	0.9996	50.19	$5.67 \cdot 10^8$	0.9997
5.0	49.43	$9.52 \cdot 10^7$	0.9993	49.95	$3.29 \cdot 10^8$	0.9996
7.5	44.53	$7.24 \cdot 10^6$	0.9993	45.25	$2.12 \cdot 10^7$	0.9996
10.0	43.55	$3.69 \cdot 10^6$	0.9998	44.91	$1.47 \cdot 104$	0.9998
15.0	45.39	$8.37 \cdot 10^6$	0.9998	50.24	$1.46 \cdot 107$	0.9993
20.0	44.98	$5.54 \cdot 10^6$	0.9999	50.02	$2.22 \cdot 10^8$	0.9994

Table 8 Statistical analysis of kinetic data (activation energy)

		AR $CaCO_3$		Insitu $CaCO_3$	
Kinetic equations		Φ	m	Φ	m
Coats–Redfern	$\bar{x}$	43.15	46.11	43.36	48.43
	s	0.16	2.41	0.39	2.60
	cv, %	0.37	5.22	0.90	5.36
Madhusudanan–Krishnan–Ninan	$\bar{x}$	43.43	46.38	44.62	48.69
	s	0.24	2.41	0.41	2.61
	cv, %	0.55	5.19	0.92	5.36
MacCallum–Tanner	$\bar{x}$	45.57	48.35	46.28	50.45
	s	0.52	2.49	0.79	2.47
	cv, %	1.14	5.15	1.70	4.90
Horowitz–Metzger	$\bar{x}$	51.98	54.82	52.39	56.18
	s	0.62	2.71	0.84	2.47
	cv, %	1.19	4.94	1.60	4.40
Contracting area	$\bar{x}$	43.15	46.11	43.36	48.43
	s	0.16	2.41	0.39	2.60
	cv, %	0.37	5.22	0.90	5.36

$\bar{x}$ = mean, s = sample standard deviation, cv = coefficient of variation

retention of carbon dioxide liberated during the decomposition reaction. This results in retardation of the forward reaction $CaCO_3 \rightleftarrows CaO + CO_2$, leading to a decrease in the over all reaction rate and thereby increase the activation energy. There is a corresponding increase in the value of preexponential factor A. This can be attributed to the kinetic compensation effect which postulates a linear relation between E and $\log A$ for a given reaction [17, 18].

* * *

We thank Director, VSSC for the kind permission to publish this work. Thanks are due to Mr. A. Natarajan for the support in SEM studies.

References

1 K. H. Stern and E. L. Weise, High Temperature Properties and Decomposition of Inorganic Salts, Part 2, Carbonates, NSRDS-NBS-30, 1969.
2 W. E. Brown, D. Dollimore and A. K. Galwey, Comprehensive Chemical Kinetics, Eds. C. H. Bamford and C. F. H. Tipper, Elsevier, New York Vol. 22, 1980.
3 P. K Gallagher and D. W. Johnson, Thermochim. Acta, 6 (1973) 67.
4 J. Zsako and H. E. Arz, J. Thermal Anal., 6 (1974) 651.
5 P. K Gallagher and D. W. Johnson, Thermochim. Acta, 14 (1976) 255.
6 Gy. Pokol and E. Pungor, Thermochim. Acta, 16 (1976) 339.
7 J. P. Elder and V. B. Reddy, J. Thermal Anal., 31 (1986) 395.
8 J. Sestak, Talanta, 13 (1966) 567.
9 K. N. Ninan and K. Krishnan, J. Spacecraft and Rockets, 19 (1982) 92.
10 A. W. Coats and J. P. Redfern, Nature (London), 201 (1964) 68.
11 P. M. Madhusudanan, K. Krishnan and K. N. Ninan, Thermochim. Acta, 97 (1986) 189.
12 J. R. MacCallum and J. Tanner, Eur. Polym. J., 6 (1970) 1033.
13 H. H. Horowitz and G. Metzger, Anal. Chem., 35 (1963) 1464.
14 V. Satava, Thermochim. Acta, 2 (1971) 2.
15 P. H. Fong and D. T. Chen, Thermochim. Acta, 18 (1977) 273.
16 W. W. Wendlandt, Thermal Methods of Analysis, 3rd Edn., Wiley, New York 1986.
17 P. D. Garn, J. Thermal Anal., 10 (1976) 99.
18 V. M. Gorbachev, J. Thermal Anal., 9 (1975) 121.

Zusammenfassung — An zwei verschiedenen Arten von Calciumcarbonat (analytisch rein bzw. in situ hergestellt aus Calciumoxalatmonohydrat) wurden thermogravimetrische Untersuchungen durchgeführt. Die Kinetik und der Mechanismus der thermischen Feststoffzersetzungsreaktionen wurde unter Anwendung integrativer Verfahren aus TG-Daten ermittelt. Auch der Einfluß experimenteller Bedingungen, wie z.B. von Aufheizgeschwindigkeit, Probenmasse und Rechenmethode wurden untersucht. Die experimentellen Bedingungen haben im untersuchten Intervall keinen sichtlichen Einfluß auf die Ergebnisse; in jedem Falle hatten die kinetischen Parameter für in situ hergestelltes Calciumcarbonat wesentlich höhere Werte. Dies wird durch die Anwesenheit von wesentlich mehr Mikroporen in dem in situ hergestellten Calciumcarbonat erklärt. Der Reaktionsmechanismus der Zersetzung wird mittels Phasengrenzreaktionen mit zylindrischer Symmetrie erklärt.